Magnetic properties of Cr-based diluted magnetic semiconductors

W. Mac and A. Twardowski
Institute of Experimental Physics, Warsaw University, 00681 Warsaw, Poland

P. J. T. Eggenkamp and H. J. M. Swagten
Department of Physics, Eindhoven University of Technology, 5600 MB Eindhoven, The Netherlands

Y. Shapira
Department of Physics and Astronomy, Tufts University, Medford, Massachusetts 02155

M. Demianiuk
Institute of Technical Physics, Wojskowa Akademia Techniczna, 00908 Warsaw, Poland
(Received 14 April 1994; revised manuscript received 24 June 1994)

We report on the magnetic properties of the Cr-based diluted magnetic semiconductors $Zn_{1-x}Cr_xSe$ and $Zn_{1-x}Cr_xS$ ($x < 0.01$). The specific heat was measured in the temperature range $1.5 < T < 10$ K and in magnetic fields up to 3 T, while the magnetization was measured at $2 < T < 40$ K and $B < 6$ T. The magnetic behavior is neither that of Brillouin paramagnets [Mn Co diluted magnetic semiconductors (DMS)] nor of Van Vleck systems (Fe DMS). It results from a strong, static Jahn-Teller (JT) distortion for the Cr ions. A simple crystal-field model, which includes the JT effect, provides an overall description of the experimental data, but some discrepancies remain.

I. INTRODUCTION

Diluted magnetic semiconductors (DMS) are mixed crystals based on classical compound semiconductors (such as CdTe, ZnSe, or InAs), in which a controlled fraction of nonmagnetic cations is replaced by magnetic ions of transition metals or rare earth metals.[1] DMS have attracted considerable attention for the last two decades, since they bridge physics of semiconductors and magnetic materials. On one hand, they still behave as typical semiconductors, but their sensitivity to magnetic field is dramatically enhanced due to the s,p-d, f exchange interaction between delocalized band electrons (s and p type) and localized d (or f) electrons of magnetic ions. Resulting giant magneto-optical effects, such as Faraday rotation or Zeeman splitting, are characteristic of DMS.[1] From the magnetic point of view, DMS represent systems of localized magnetic moments (associated with magnetic ions) randomly distributed in a nonmagnetic host lattice and coupled by antiferromagnetic (AF) long-ranged d-d exchange interaction.[2,3] Depending on the concentration of magnetic ions and the temperature range DMS reveal paramagnetic, spin-glass, or antiferomagnetic behavior.

The paramagnetic behavior of DMS depends crucially on the magnetic ion. Substitutional Mn ions in II-VI compounds represent the simplest situation. The electronic configuration of Mn^{++} is d^5, and the ground level of the ion at zero magnetic field is a degenerate multiplet with vanishing orbital momentum (L=0, S=5/2). The magnetic moment of the ion results solely from the spin, so that Mn-based DMS behave like typical Brillouin paramagnets.[2,3] The same type of paramagnetism is observed for Co-based DMS.[4] The situation for Fe DMS is completely different. In this case (d^6 configuration), the orbital momentum is nonvanishing (L=2, S=2) and the ground state is a singlet. Consequently, a magnetic moment for the Fe ion can only be induced by a magnetic field, so that Fe DMS show typical Van Vleck–type paramagnetism.[5]

Until now most of the research on DMS was devoted to DMS containing Mn, Co, or Fe. Only recently a new class of DMS based on Cr was synthesized. Preliminary results reported for $Zn_{1-x}Cr_xSe$ show that these materials are markedly different from all the other DMS.[6] The most striking difference is the ferromagnetic p-d exchange between Cr ions and valence band electrons,[7] whereas in all DMS which have been studied earlier this interaction was always AF.[1] Ferromagnetic p-d exchange may also result in ferromagnetic coupling between Cr ions. From the magnetic point of view the Cr^{++} ion represents an intermediate case between Brillouin and Van Vleck paramagnetisms: the ground state is a multiplet (actually a "semidoublet" as discussed later) but excited states are close enough to contribute to the magnetic properties. Moreover, the Cr ion is strongly influenced by the Jahn-Teller (JT) effect,[8,9] which is rather unimportant for Mn, Co, and Fe. We, therefore, thought it worthwhile to study the magnetic properties of Cr DMS in some detail.

In this paper, we report results of specific heat and magnetization for two materials: $Zn_{1-x}Cr_xSe$ and $Zn_{1-x}Cr_xS$. The data are interpreted using a simple crystal-field model, but including the JT effect. The paper is organized as follows. After a discussion of experimental details in Sec. II, the experimental data are

0163-1829/94/50(19)/14144(11)/$06.00

presented in Sec. III. The crystal-field model is presented in Sec. IV and is applied to the present data in Sec. V. The main conclusions are summerized in Sec. VI.

II. EXPERIMENT

The crystals were grown by the modified Bridgman technique. $Zn_{1-x}Cr_xSe$ was grown of high purity ZnSe and pure metallic Cr. Occasionally, CrSe was also used. In the case of $Zn_{1-x}Cr_xS$ the crystals were grown of ZnS and pure Cr. Single phase crystals were obtained only for rather low Cr concentrations, $x < 0.01$. Attempts to grow crystals with higher x resulted in precipitations of Cr_ySe_z (or Cr_yS_z). Only single phase samples were used in the present study. The composition of the samples was checked by atomic absorption and by chemical analysis. Due to the low x values, the accuracy of these measurements was only 10–20 % of the actual x. For some of the samples we used the magnetization data to compare the Cr content of different samples. Such a procedure was justified by the fact that magnetization scales with x, as described in Sec. III B. The values of x resulting from the magnetization calibration are in tolerable agreement with the microprobe results.

The crystalline structure of the crystals was analyzed by x-ray diffraction. $Zn_{1-x}Cr_xSe$ crystals were found to be cubic. In some cases the $Zn_{1-x}Cr_xSe$ samples were composed of grains, misoriented relative to each other by about 2–3 degrees. The $Zn_{1-x}Cr_xS$ crystals revealed "hexagonal" structure (mixed polytypes of cubic and hexagonal ZnS).

The specific heat was measured using the standard heat pulse technique. Data were taken in the temperature range 1.5–15 K, and in magnetic fields B up to 3 T. Due to the low concentration of Cr, rather large samples (about 0.3 – 0.5 g) were necessary.

The magnetization was measured using a superconducting quantum interference device magnetometer in the temperature range 2–40 K and in magnetic fields up to 6 T. All the magnetization data were corrected for diamagnetism of the host lattice [$\chi_d^{ZnSe} = -3.2$ emu/g, $\chi_d^{ZnS} = -3.9$ emu/g (Ref. 10)].

III. RESULTS

A. Specific heat

The magnetic contribution C_m to the total heat capacity C_{tot} of the sample was evaluated as the difference: $C_m = C_{tot} - C_{latt}$, where C_{latt} is the heat capacity of the nonmagnetic lattice. In most cases C_{latt} was approximated by the specific heat of the host material, i.e., ZnSe or ZnS. It is known that such a procedure can substantially overestimate C_{latt}, in particular if there is a pronounced mass difference between the nonmagnetic cation of the host and the magnetic ion.[11] However, in our case the mass difference between Cr and Zn is relatively small. Moreover, the Cr concentrations are small, so that the approximation $C_{latt} \approx C_{ZnSe}$ (or C_{ZnS}) is expected to be valid.

Representative results of C_m at zero magnetic field are shown in Fig. 1, both for $Zn_{1-x}Cr_xSe$ (x=0.004) and for $Zn_{1-x}Cr_xS$ (x=0.004 and 0.006). We notice the typical onset of a Schottky-type anomaly, indicating the existence of an energy gap (of the order of few K) between the ground and the excited levels. A similar situation was encountered in the case of Fe-based DMS.[5] Application of a magnetic field results in a strong increase of C_m (Figs. 2 and 3), in contrast with Fe-DMS, but similar to Mn- and Co-based DMS.[2–4] The observed field dependence shows that the ground state is a multiplet, since a split multiplet provides a series of levels that can be thermally populated, thereby giving rise to an increase of the specific heat.

The data for $Zn_{1-x}Cr_xSe$ and $Zn_{1-x}Cr_xS$ are qualitatively the same. A slight shift to lower temperatures of the C_m curve of $Zn_{1-x}Cr_xS$ relative to those for ZnSe can be observed. This shift suggests a smaller energy gap between the ground and the excited levels of $Zn_{1-x}Cr_xS$. We will return to this point later.

The data for $Zn_{1-x}Cr_xSe$ were obtained for unoriented samples, because single crystals of a suitable size were not available. In the case of $Zn_{1-x}Cr_xS$ the magnetic field was parallel to the sixfold axis (corresponding to the ⟨111⟩ axis in a cubic crystal).

B. Magnetization

The magnetization of $Zn_{1-x}Cr_xSe$ was measured on oriented samples (of mass about 0.02 g) for magnetic field perpendicular to three principal crystallographic directions ⟨100⟩, ⟨110⟩, and ⟨111⟩. Figure 4 shows representative results for $\mathbf{B} \parallel \langle 100 \rangle$ at different temperatures. At the lowest temperatures the magnetization varies strongly with B, although no saturation is observed despite the rather low x. This behavior is in

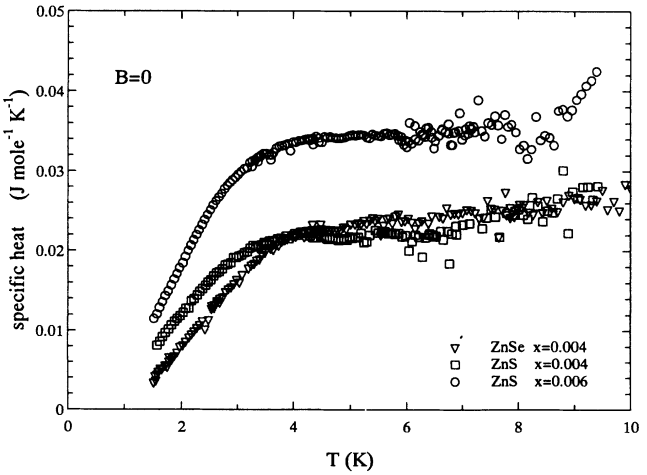

FIG. 1. Magnetic contribution to the specific heat of $Zn_{1-x}Cr_xSe$ (x = 0.004) and $Zn_{1-x}Cr_xS$ (x = 0.004,0.006) in the absence of a magnetic field.

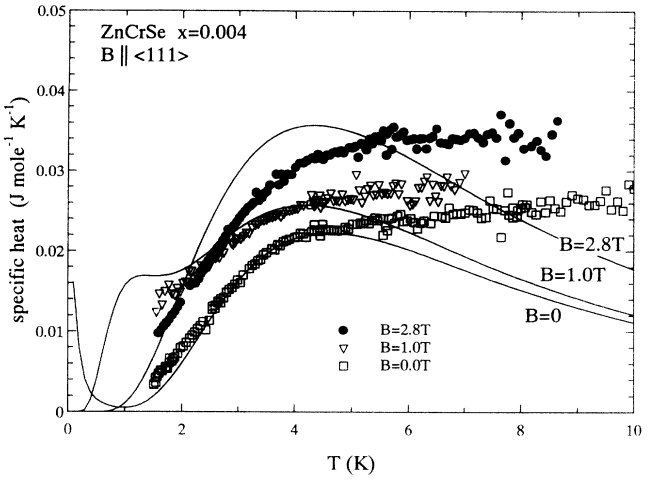

FIG. 2. Magnetic specific heat of $Zn_{1-x}Cr_xSe$ ($x = 0.004$) for $\mathbf{B} = 0$, 1, and 2.8 T. The field $\mathbf{B}$ is not oriented along any specific direction. The solid lines show the calculated specific heat for $\mathbf{B} \parallel \langle 111 \rangle$, as described in the text.

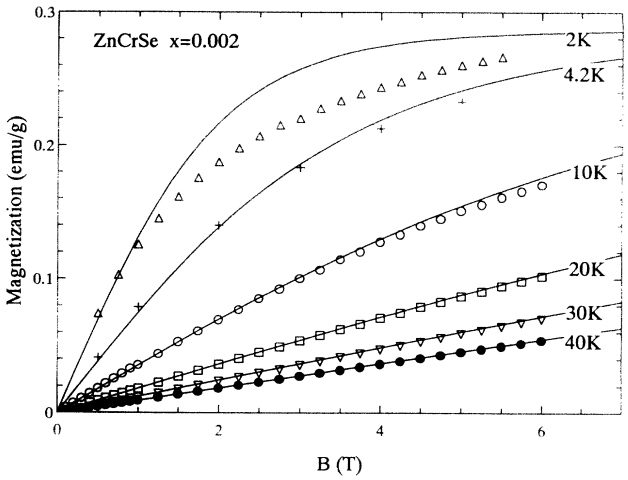

FIG. 4. Magnetization of $Zn_{1-x}Cr_xSe$ ($x = 0.002$) as a function of magnetic field ($\mathbf{B} \parallel \langle 100 \rangle$) at various temperatures. The lines show the magnetization calculated according to the EQ model, as discussed in the text. The concentration x was slightly adjusted to the value 0.0022 providing the correct absolute magnetization value for $T > 10$ K.

contrast with that of Mn and Co DMS, and it reflects the presence of the excited states close to the ground multiplet. We also notice a strong variation of M with temperature; in contrast to Van Vleck paramagnets (e.g., Fe-DMS) whose magnetization is temperature independent at low T.[5]

Figure 5 shows that the magnetization is anisotropic (depends on the B direction), in particular at the highest fields. On the other hand, at the lowest fields ($B < 1$ T, linear response range) the magnetization is isotropic. The easy magnetization axis is $\langle 100 \rangle$, whereas both $\langle 111 \rangle$ and $\langle 110 \rangle$ behave like hard axes. Only a small difference is observed between the magnetization for the $\langle 110 \rangle$ and $\langle 111 \rangle$ directions. The anisotropy decreases with increasing temperature. At temperatures higher than 20 K the magnetization is practically isotropic (the observed difference is below experimental accuracy).

The shape of both magnetization and specific heat does not depend on Cr concentration, as exemplifed in Fig. 6. Part (a) of this figure shows that the specific heat of two $Zn_{1-x}Cr_xS$ samples differ only by a constant multiplicative factor (1.545 in this case). A similar situation is encountered for the magnetization of $Zn_{1-x}Cr_xSe$ [Fig. 6(b)]. Such a scaling with concentration (implying

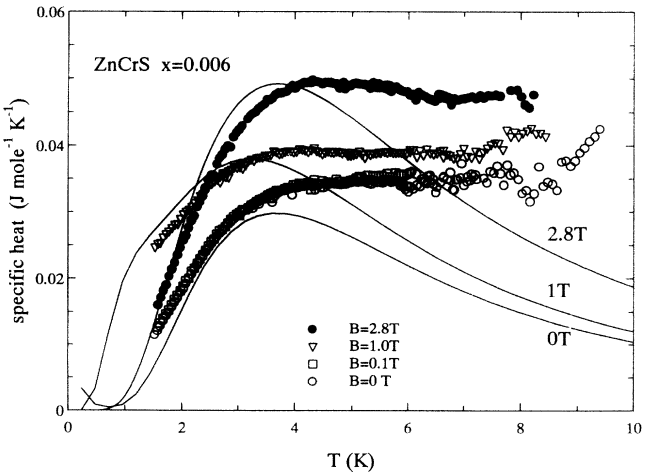

FIG. 3. Magnetic specific heat of $Zn_{1-x}Cr_xS$ ($x = 0.006$) for $\mathbf{B} = 0$, 0.1, 1, and 2.8 T ($\mathbf{B}$ parallel to sixfold axis) The solid lines show the calculated specific heat for a cubic crystal with $\mathbf{B} \parallel \langle 111 \rangle$, as described in the text. The curve for $\mathbf{B} = 0.1$ T is practically the same as for $\mathbf{B} = \mathbf{0}$ and, therefore, is not shown.

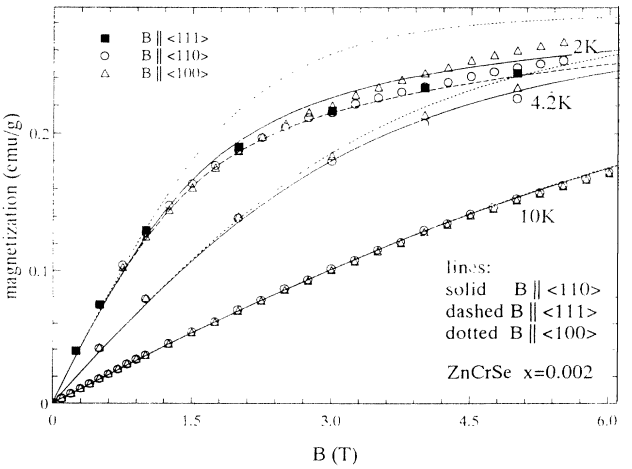

FIG. 5. Anisotropy of the magnetization of $Zn_{1-x}Cr_xSe$ ($x = 0.002$) at various temperatures. The lines show the magnetization calculated according to the EQ model, as discussed in the text. The concentration x was slightly adjusted to the value 0.0022 providing the correct absolute magnetization value for $T > 10$ K.

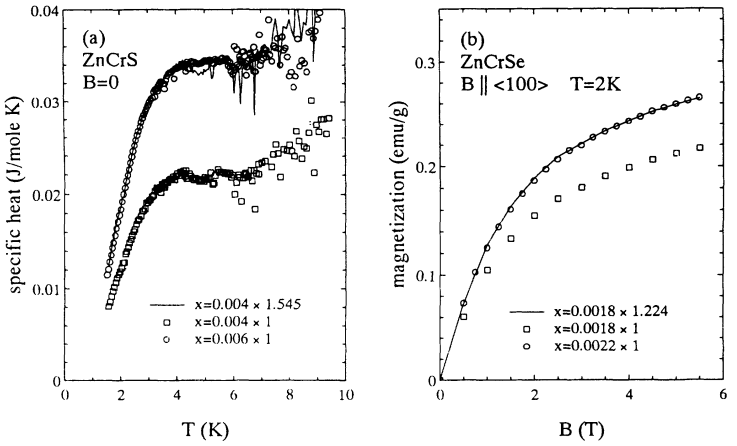

FIG. 6. Scaling of (a) the specific heat of ZnCrS and (b) the magnetization of $Zn_{1-x}Cr_xSe$ with concentration x of Cr ions. The line in (a) was obtained by multiplying the specific heat for $x = 0.004$ by 1.545. The line in (b) was obtained by multiplying the magnetization for $x = 0.0018$ by a factor of 1.224.

an independence of the shape of a given thermodynamic quantity on concentration) means that the interaction between Cr ions is unimportant here.[2,3] In our case, this behavior results from the small x values of our crystals. For instance, for $x = 0.005$ about 94% of the ions have no nearest magnetic neighbors, so that the d-d exchange interaction, if any, can be expected for only 6% of the ions. In such a case, no conclusions about the strength of the interaction between nearest neighbour Cr ions can be obtained from the data. Therefore, the model which assumes a system of noninteracting Cr ions should provide a resonable description of the present data. In such a model any thermodynamic quantity is a product of a single ion quantity multiplied by the number of the ions. Consequently, the magnetization or specific heat of a sample with Cr concentration x_1 can be obtained from the data of the other sample with x_2 by multiplying the data by the x_1/x_2 ratio. For the samples shown in Fig. 6(a) the Cr concentration, as obtained from microprobe analysis, was $x_1 = 0.006$ and $x_2 = 0.004$ so one should expect a scaling factor of 1.5. The actual scaling factor is 1.545 in this case, which is in very good agreement with the concentration ratio, especially keeping in mind the rather poor accuracy of the microprobe analysis for such a low x. The magnetization data presented in Fig. 6(a) show that the scaling factor for the two samples is 1.22, which we believe reflects the actual concentration ratio. The relative Cr concentration determined in this way is much more accurate than the value resulting from the conventional methods of x determination (microprobe or chemical analysis), since the latter methods are not precise enough for low x. The final x values given in Fig. 6(b) (0.0018 and 0.0022) were chosen to provide the best fit of the magnetization data for $T > 10$ K by the model described in Sec. IV C. We notice that these values are in agreement with the microprobe results, within the experimental accuracy.

IV. THE MODEL

A. Energy structure of isolated Cr^{++} ion

To describe the Cr^{++} (d^4) ion we generally follow the crystal-field model developed by Vallin *et al.*[8] It was shown that in order to describe the Cr d level in a cubic lattice one needs to include in the Hamiltonian not only a tetrahedral crystal-field, spin-orbit interaction and the magnetic field, but also the JT effect. This effect was found to result in a static, tetragonal distortion of the Cr center.[8,9] Therefore, the full Hamiltonian can be written in the form

$$\mathcal{H} = \mathcal{H}_{\rm cf} + \mathcal{H}_d + \mathcal{H}_{\rm so} + \mathcal{H}_B, \qquad (1)$$

where $\mathcal{H}_{\rm cf} = B_4(O_4^0 + 5O_4^4)$ describes the tetrahedral (cubic) crystal field[12] (the operators O_b^a are defined in Ref. 12), $\mathcal{H}_d = B_2^0 O_2^0 + B_4^0 O_4^0$ describes the tetragonal static Jahn-Teller distortion, $\mathcal{H}_{\rm so} = \lambda \mathbf{LS}$ is the spin-orbit term [$\mathbf{L} = (L_x, L_y, L_z)$ is the orbital angular momentum operator and $\mathbf{S} = (S_x, S_y, S_z)$ is the spin operator], and $\mathcal{H}_B = \mu_B(\mathbf{L} + 2\mathbf{S})\mathbf{B}$ is the Zeeman energy and μ_B is the Bohr magneton.

The order of the four terms on the right-hand side of Eq. (1) is significant: each succesive term represents a progressively weaker interaction.

We recall that the ground term of the Cr^{++} free ion is an orbital and spin quintet ^5D with $L = 2$ and $S = 2$, similar to the case of the Fe^{++} ion[13–15] (see Appendix).

The crystal field splits the ground ^5D term into an orbital triplet $^5T_2$ and an orbital doublet ^5E [Fig. 7(a)]. The JT tetragonal distortion then splits the $^5T_2$ term into an orbital doublet ^5E and an orbital singlet $^5B_2$, whereas the ^5E doublet is split into orbital singlets $^5B_1$ and $^5A_1$.

Spin-orbit interaction yields further splittings.[8] In particular, the ground state $^5B_2$ is split into a semidoublet Γ_1, Γ_2, a doublet Γ_5, and a singlet Γ_4. The semidoublet Γ_1, Γ_2 consists of two levels with a tiny energy separation, only ~ 0.2 cm^{-1}.

It must be noted that the low energy structure of the Cr ion would have been completely different had the JT distortion been absent. In that case, the ground state would have been a singlet (instead of a semidoublet), resulting in a typical Van Vleck-type paramagnetism of the Cr ion. Application of a magnetic field lifts the degeneracy of the remaining multiplets and mixes some of the levels.

In the present work, we calculated the energy level

TABLE I. Experimental spectroscopic data for Cr^{++} in ZnSe and ZnS. All energies are in cm^{-1}.

Crystal	$\Gamma_1\Gamma_2 \rightarrow \Gamma_5$ transition (FIR)	JT splitting ($= 3E_{JT}$)	Zero phonon line (ZPL)
ZnSe	7.43[a]	1650[a]	4975[a]
		1110[b]	
ZnS	5.53[a,c]	1725[a]	5224[a]

[a]Reference 8.
[b]Reference 16.
[c]Reference 17.

scheme of the Cr^{++} ion by a numerical diagonalization of the full 25 × 25 Hamiltonian (1) matrix (see Appendix). Thus all interactions were taken into account without any approximations. The Hamiltonian matrix is parametrized by four parameters: B_4, B_2^0, B_4^0, and λ. These parameters are evaluated by comparing the calculated energies with experimental data. For this evaluation we used the energies of optical transitions between the ground semidoublet (Γ_1, Γ_2) and (1) the first excited, spin-orbit split Γ_5 state (denoted as the FIR transition), (2) the lowest Γ_5 level of the ^5E state, originating

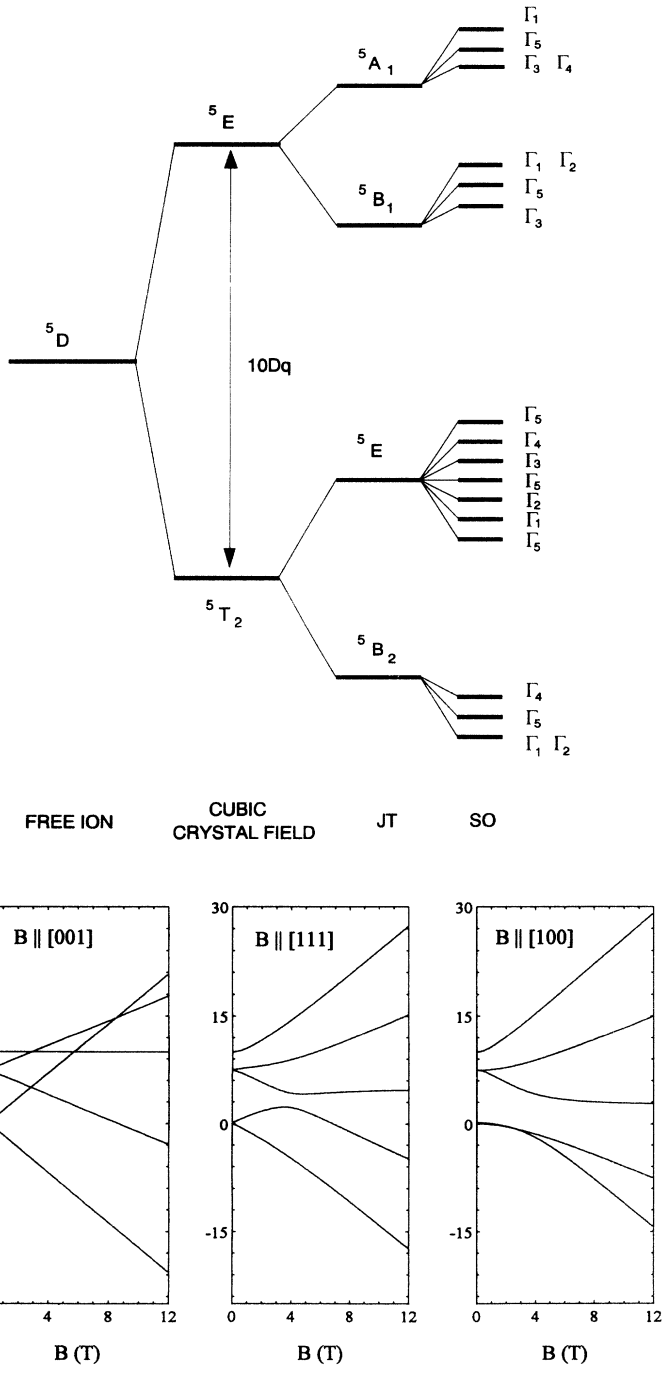

FIG. 7. Energy levels of the Cr^{++} ion, (a) energies in the absence of magnetic field (energy distances are not to scale), (b) the five lowest-energy Cr^{++} levels, calculated as a function of magnetic field **B** along the [001], [111], and [100] directions. The static Jahn-Teller distortion is along [001]. The parameters used correspond to Cr^{++} in ZnSe (Table II).

TABLE II. Parameters Dq, B_4^0 ($B_2^0 = 5B_4^0$), and λ used in our calculations, together with calculated transition energies. All energies are in cm^{-1}.

Crystal	Dq	B_4^0	λ	FIR	JT splitting	ZPL
ZnSe	−494.25	−17.14	+84.8	7.42	1648	4975.2
ZnS	−520.0	−17.8	+77.0	5.52	1729	5225

from $^5T_2$ crystal-field term (denoted as JT splitting), (3) the lowest Γ_3 level of the $^5B_1$ level, originating from the ^5E crystal-field term [denoted as the zero phonon line (ZPL)].

These transitions were observed for ZnSe and ZnS. Their energies are tabulated in Table I. The parameters of the Hamiltonian were chosen to provide the best matching between the calculated and measured energies of Table I. The resulting parameters are collected in Table II, which also gives the transition energies calculated with these parameters. We note that the ZPL energy is approximately $10Dq(= 120B_4)$. Analysis of the IR absorption results suggests that the JT splitting of the ^5E, crystal-field term, is very small.[8] We, therefore, arbitrarily set this splitting to zero, which corresponds to the relation $B_2^0 = +5B_4^0$ [cf. Eq. (A2)]. With this approximation the JT splitting of the $^5T_2$ term (energy 2) roughly equals $105B_4^0$, if the spin-orbit correction is neglected. The magnetic properties are dominated by the lowest levels Γ_1, Γ_2, Γ_5, and Γ_4 (resulting from the splitting of $^5B_2$) and are not sensitive to the higher energy levels, so that these higher energy levels need not be very precisely recovered. For instance, decreasing Dq by 10% and readjusting the spin-orbit parameter λ, to get the same energy gap between Γ_1, Γ_2, and Γ_5, leaves the magnetization practically unchanged.

Using the parameters in Table II we calculated the energy levels of Cr^{++} ion in ZnSe and ZnS, with **B** along the principal directions. Figure 7 shows examples of the results for the levels resulting from the splitting of the $^5B_2$ level. At **B**=**0** there is a small (≈ 0.14 cm^{-1}) splitting between the levels Γ_1 and Γ_2 of the semidoublet. The in-field calculated results reveal a strong anisotropy of the energy structure, i.e., dependence on field direction. The strongest splittings occurs for **B** parallel to the distortion axis (**B** ∥ [001]). We denote this configuration as the "0°" configuration. On the other hand for **B** perpendicular to the distortion axis (**B** ∥ [100], "90°" configuration) the splitting of the semidoublet Γ_1, Γ_2 is very small. For the other field directions (denoted as "α°" configuration, where α is the angle between field and distortion direction) we find intermediate splittings.[24]

B. Magnetic properties of a single Cr^{++} ion

The anisotropy of the energy-level structure is reflected in the magnetic moment and specific heat of the Cr^{++} ion. The average magnetic moment per Cr ion (in units μ_B) is the expectation value of the magnetic moment operator $\mathbf{M} = \mathbf{L} + 2\mathbf{S}$

$$\langle \mathbf{M} \rangle = \frac{\sum \langle \Psi_i \mid \mathbf{L} + 2\mathbf{S} \mid \Psi_i \rangle e^{\frac{-E_i}{k_B T}}}{\sum e^{\frac{-E_i}{k_B T}}}, \tag{2}$$

where k_B is the Boltzman constant and index i refers to the ith state.

The magnetic specific heat per Cr ion is given by

$$C_m = \frac{k_B}{(k_B T)^2}(\langle E^2 \rangle - \langle E \rangle^2), \tag{3}$$

where $\langle E^n \rangle$ is the expectation value of the nth power of the energy operator.

The results of the calculations are shown in Fig. 8. For the magnetization the distortion direction, denoted as [001], is the easy magnetization axis (0° configuration), whereas the perpendicular direction corresponds to hard

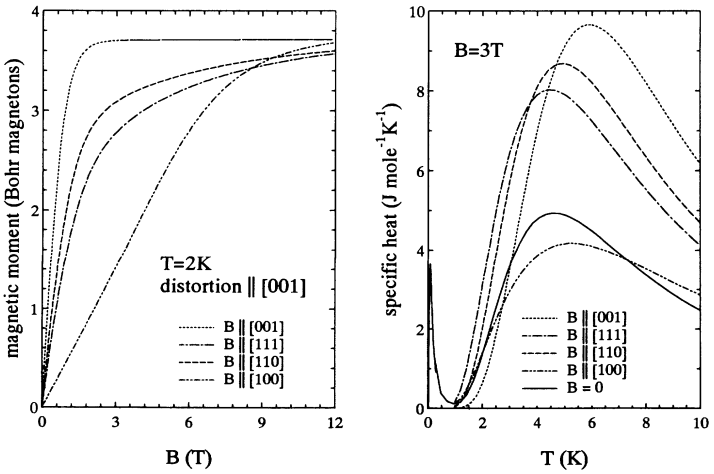

FIG. 8. Calculated magnetic moment and specific heat of a single Cr center in ZnSe distorted along the [001] direction for different orientations of the magnetic field: **B** ∥ [001], [101], [111], and [100], (a) The **B** dependence of the magnetization at 2 K, (b) the T dependence of the specific heat at 3 T.

magnetization axis (90° configuration). In general, when the angle α between the field and the distortion axis is smaller the magnetic moment is larger, at least for not very strong magnetic fields ($B < 6$ T). This is exemplified by the [101] and [111] directions, for which $\alpha = 45°$ and $\alpha = 54.7°$, respectively. The saturation value of the magnetic moment is slightly lower than expected for spin S=2 (about 3.7, instead 4.0), which reflects the negative contribution of orbital momentum to the total magnetic moment (we recall that for Fe^{++} the orbital contribution was of the same order of magnitude, but with opposite sign[5,18]).

The magnetic specific heat shows a strong increase with magnetic field, resulting from the splitting of the ground semidoublet Γ_1, Γ_2. Only for **B** perpendicular to the distortion axis, for which the splitting of the semidoublet is very small (at low fields, $B < 4$ T), is the increase of the specific heat rather small. In fact, the latter increase is mainly due to the excited states approaching the ground state, rather than to the splitting of the semidoublet [cf. Fig. 7(b)]. We note that the peak in zero field C_m, at about 0.085 K, reflects small splitting of the ground state (mentioned above).

C. Magnetic properties of the crystals of Cr DMS

So far we discussed a single Cr center with a JT distortion along the [001] direction. For a real crystal there are three equivalent ⟨001⟩ directions: [100], [010], and [001], which means that there are, in fact, three types of tetragonally-distorted centers. We denote a center for which the distortion axis is along [100] as A center and similarly B center for [010] distortion and C center for [001] distortion (Fig. 9). The results in Figs. 7 and 8, therefore, correspond to those for a C center. In the absence of a magnetic field the three types of centers are equivalent. However for $\mathbf{B} \neq 0$ different centers are no longer equivalent since, in general, the angle α between **B** and the distortion axis is different for the A, B, and C centers. Only for **B** along a high symmetry direction does the number of nonequivalent centers reduce to two or one. In particular for **B** ∥ [100], center A represents the 0° configuration (**B** ∥ distortion axis), whereas centers B and C are both in 90° configuration (**B** ⊥ distortion axis). For **B** ∥ [011] center A is in the 90° configuration and both B and C are in the 45° configuration. The simplest situation is encountered for **B** ∥ [111], for which A, B, and C are equivalent (54.7° configuration) (Fig. 9).

The different centers A, B, and C were indeed observed in a far infrared absorption experiment on $Zn_{1-x}Cr_xSe$.[21] In particular the energy levels of the 90° configuration were visible for **B** ∥ ⟨100⟩ and **B** ∥ ⟨110⟩, but they were absent for **B** ∥ ⟨111⟩.

A macroscopic quantity, such as the magnetization or the specific heat, is, therefore, some average of the contributions from different centers. The difficulty is in assigning proper weights to the contributions from the three types of centers. In the absence of a magnetic field, all the centers are equivalent and, therefore, there are equal numbers of A, B, and C centers. However, this may not be the case when a magnetic field is present. A magnetic field distinguishes between different centers, so that a variation of the numbers of the three types of centers may occur, as **B** varies. We consider here two extreme models. The first one, called "nonequilibrium" (NEQ), assumes that there is no readjustment of the numbers of the various centers, i.e., the numbers at any **B** remain the same as at **B**=**0**. In other words, we assume infinite potential barriers between different centers. In the opposite extreme there are no barriers at all. This latter extreme case will be called the "equilibrium" model (EQ). The populations of the various centers in this case are governed by the equilibrium condition.

In the NEQ model any thermodynamic quantity X is a simple average over the three centers:

$$\langle X\rangle_{A,B,C} = \tfrac{1}{3}\langle X\rangle_A + \tfrac{1}{3}\langle X\rangle_B + \tfrac{1}{3}\langle X\rangle_C, \qquad (4)$$

where index A denotes average for the center A, etc. Figure 10(a) shows the macroscopic magnetization calculated using the NEQ model. A strong anisotropy is observed, but the sense of this anisotropy is opposite to that in Fig. 8 (which corresponds to a center C only). The ⟨001⟩ direction is now the hard axis, since only one center is in 0° configuration, while two of them are in

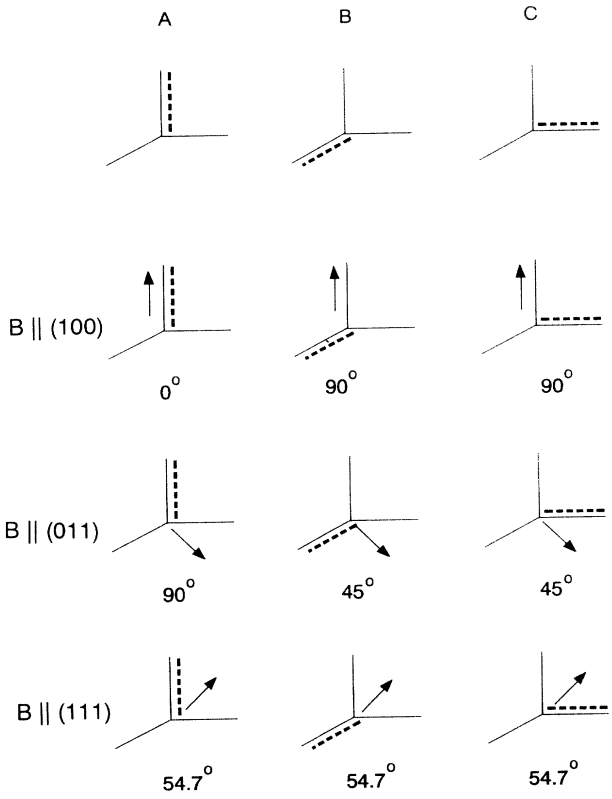

FIG. 9. Configuration of different Cr centers (A, B, and C) for different magnetic field directions (represented by arrows). The distortion axis for each Cr center is shown by a dashed line. The numbers correspond to the angle between the magnetic field and the distortion axis.

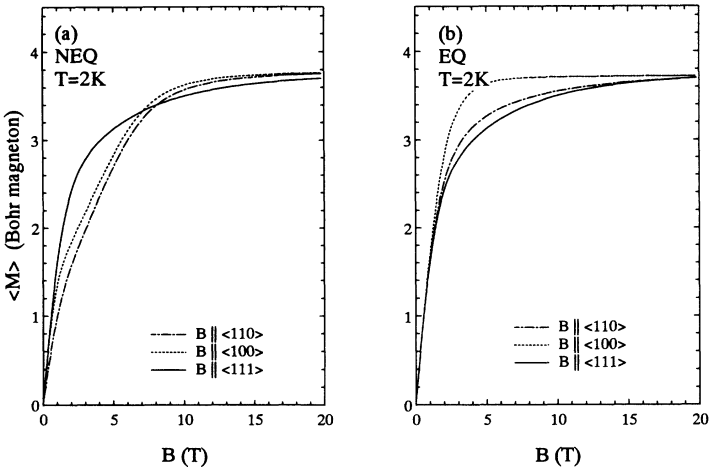

FIG. 10. Average magnetic moment per Cr ion in $Zn_{1-x}Cr_xSe$, calculated according to the equilibrium (EQ) and nonequilibrium (NEQ) models for different magnetic field orientations: $\mathbf{B} \parallel \langle 100\rangle$, $\langle 111\rangle$, and $\langle 110\rangle$. Unlike Fig. 8, all three types of centers (A, B, and C) are present.

90° configurations. On the other hand, for $\mathbf{B} \parallel \langle 110\rangle$ there is only one 90° center, but two other centers are in the 45° configuration, so that the magnetization for this direction is larger than for $\mathbf{B} \parallel \langle 001\rangle$. In the case of $\mathbf{B} \parallel \langle 111\rangle$ all the centers are in the 54.7° configuration, and although they are less responsive than the centers in the 45° or 0° configurations, their statistical weight is tripled. As a result the average magnetization is largest for $\mathbf{B} \parallel \langle 111\rangle$ when $\mathbf{B} < 7$ T (for $\mathbf{B} > 7$ T anisotropy is reversed and $\langle 111\rangle$ becomes the hard axis).

The specific heat calculated in the NEQ model for $\mathbf{B}$=3 T is displayed in Fig. 11(a). The largest C_m occurs for $\mathbf{B} \parallel \langle 111\rangle$, similar to the magnetization. Slight differences in the energy gap between the ground and the first excited state for different field directions are reflected by the different positions of C_m maxima.

In the NEQ model the three types of centers are viewed as independent thermodynamic systems. In the EQ model, on the other hand, all centers are in one thermodynamic system. In this case the probability of occupation of a given level depends on its energy, and the mean value of the quantity X is given by

$$\langle X\rangle_{A,B,C} = \frac{\sum \langle \Psi_i \mid X \mid \Psi_i\rangle e^{\frac{-E_i}{k_B T}}}{\sum e^{\frac{-E_i}{k_B T}}} = \langle X\rangle_A \frac{Z_A}{Z} + \langle X\rangle_B \frac{Z_B}{Z} + \langle X\rangle_C \frac{Z_C}{Z}, \quad (5)$$

where the summation runs over states of the centers A, B, and C. Here Z_n is the partition function of a center of type n

$$Z_n = \sum e^{\frac{-E_i^n}{k_B T}}, \quad (6)$$

where now the summation is only over the energies of that center. The total partition function of the system is $Z = Z_A + Z_B + Z_C$.

Obviously in such a model the centers with the lowest ground state provide the dominant contribution to the mean value $\langle X\rangle$. Since the largest decrease of the ground state energy with $\mathbf{B}$ occurs for the 0° configuration [Fig. 7(b)], this configuration will dominate the mean value

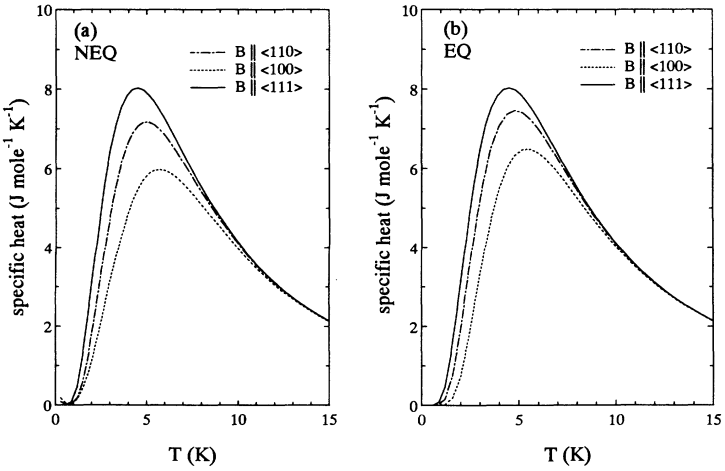

FIG. 11. Specific heat of $Zn_{1-x}Cr_xSe$ calculated according to EQ and NEQ models for different magnetic field orientations: $\mathbf{B} \parallel \langle 100\rangle$, $\langle 111\rangle$, and $\langle 110\rangle$ and $\mathbf{B} = 3$ T.

($Z_C > Z_B, \quad Z_A$). Consequently, the $\langle 001 \rangle$ direction becomes the easy magnetization axis in the EQ model, as shown in Fig. 10(b). The anisotropy dependence on direction for $\mathbf{B} < 7$ T is reversed relative to that in the NEQ model.

Examples of the specific heat calculated in the EQ models shown in Fig. 11(b), which is for $\mathbf{B} = 3$ T. In this field the energy gap between the ground state and the first excited level is practically the same for 45° and 54.7° configurations. Moreover it is about two times smaller than for the 0° configuration case [see Fig. 7(b), where $\mathbf{B} \parallel [001]$ corresponds to 0° and $\mathbf{B} \parallel [111]$ to 54.7°], which makes the contribution to the specific heat of the 0° centers relatively unimportant. Consequently, the difference between the EQ and NEQ models is much less pronounced (Fig. 11).

V. DISCUSSION

As already noted (Sec. III), no effects of the Cr-Cr interaction are observed in our crystals. Therefore, the magnetic behavior should result from isolated Cr^{++} ions, whose properties were presented in the previous section. The macroscopic magnetization $\mathbf{M}_m$ and the specific heat C_m can then be written in the form

$$\mathbf{M}_m = \mu_B \langle \mathbf{M} \rangle x N_{\mathrm{Av}} / m_{\mathrm{mole}} \tag{7}$$

and

$$C_m = c_m x N_{\mathrm{Av}}, \tag{8}$$

where $N_{\mathrm{Av}} = 6.022 \times 10^{23}$ is Avogadro's number, m_{mole} is mass of the $Zn_{1-x}Cr_xSe$ ($Zn_{1-x}Cr_xS$) molecule and $\langle \mathbf{M} \rangle$, c_m are calculated according Eq. (4) or Eq. (5). Before presenting a quantitative analysis we note that at high temperatures (roughly $T > 15$ K) both NEQ and EQ models give the same results for $\mathbf{M}_m$ and C_m to within 1%. However, at the lowest temperatures only the EQ model predicts the sign of the magnetization anisotropy observed experimentally (cf. Figs. 5 and 9). We, therefore, limit our considerations to this model.

The calculations with the EQ model were done using the parameters in Table II. No fitting was performed, except for a slight adjustement (about 10%) of the actual Cr concentration x, to obtain the best matching with experiment. This adjustment was within the accuracy of the x determination (see Sec. II).

The results of the specific heat calculations are shown in Figs. 2 and 3. The basic features of the experimental specific heat, such as the onset of a Schottky-type anomaly and the strong dependence on magnetic field, are recovered. Some deviation is observed for $T > 5$ K. We recall that a similar discrepancy in the high temperature part of specific heat was observed for $Zn_{1-x}Fe_xSe$ and $Zn_{1-x}Fe_xS$.[19,20] It may be that there are some additional states not taken into account in our model (including some centers different than Cr).

For $Zn_{1-x}Cr_xSe$, there is a reasonable matching of the calculations and the in-field data, although the sample was not oriented so that the calculations for $\mathbf{B} \parallel \langle 111 \rangle$ should be regarded only as an example.

In the case of the magnetization (Figs. 4 and 5), the EQ model provides an excellent description of the high temperature data ($T \geq 10$ K). However, at low temperatures only the general behavior of magnetization is recovered. The model predicts that the $\langle 100 \rangle$ directions are the easy magnetization directions, and also that $M_{\langle 110 \rangle} \approx M_{\langle 111 \rangle}$. Although the temperature dependence of the magnetization anisotropy is also in agreement with experiment (less than 1% for $T > 15$ K), its magnitude is too large at low T (Fig. 5). In addition, the calculated magnetization for $\mathbf{B} \parallel \langle 100 \rangle$ saturates too quickly (Fig. 4). This discrepancy cannot be accounted for by a slight misorientation of $\mathbf{B}$ (as may be the case for crystals possessing a grain structure). There are then two possible explanations of the discrepancy: either the energy structure is calculated incorrectly or the procedure of averaging over Cr centers of different type is incorrect. In the first case, one expects a poor matching with experiment at any temperature, not only at low T (although the difference should be largest at the lowest temperatures). Moreover, the calculated energy structure recovers the FIR optical transitions observed experimentally in $Zn_{1-x}Cr_xSe$ (Ref. 21) and $Zn_{1-x}Cr_xS$.[22] We, therefore, believe that the main problem with the calculations lies in the method of averaging over different Cr centers.

The fundamental question is whether the system is in a true thermal equilibrium or is in a state in which the distribution of centers at $\mathbf{B} \neq 0$ is intermediate between the distribution at $\mathbf{B} = 0$ and that in equilibrium. In the intermediate case the magnetization should be somewhere in between the EQ and NEQ results and it may vary with time. Experimentally, no time dependence of the magnetization was observed (within about 0.5%) for times between 1 min and 10 h. The absence of time dependence suggests that either the system reaches the equilibrium very quickly or very slowly. In the first case, the EQ model should be appropriate. In the second case, the NEQ model should apply. However, as mentioned, both models are inadequate, at least at low T. The faster-than-observed saturation of the calculated $\langle 100 \rangle$ magnetization indicates that the 0° configuration is overestimated in the calculations. Thus there must be some mechanism that prevents the Cr centers in our samples from turning into the 0° configuration. A possible cause is a uniaxial stress which may be present in the crystal. Such a stress would favor a particular direction for the JT distortion in the crystal, thus creating additional energy barriers and consequently yielding a kind of intermediate distribution of the Cr centers. Following this reasoning one could propose a "nonequilibrium" distribution which is intermediate between the NEQ model (representing those centers that are frozen due to additional energy barriers) and EQ model (corresponding to "normal," unfrozen centers). Thus far we refrained from pursuing this approach, since no information is available about the existing energy barriers. The experiments under uniaxial stress should be helpful in understanding this problem.

VI. CONCLUSIONS

The measured specific heat and magnetization of $Zn_{1-x}Cr_xSe$ and $Zn_{1-x}Cr_xS$ show a magnetic behavior typical for a quantum system with a degenerate (or "semidegenerate") ground level, separated by a small energy gap from the excited states. In this respect Cr DMS can be regarded as systems which are intermediate between Brillouin paramagnets (such as Mn and Co DMS) with a multiplet ground level separated by a large gap from the excited states, and Van Vleck-type paramagnets (such as Fe DMS) with a singlet ground state. A simple crystal-field model which takes into account (1) the tetrahedral crystal field, (2) a static, tetragonal Jahn-Teller distortion, and (3) spin-orbit interaction, recovers the basic experimental features. The importance of the Jahn-Teller distortion cannot be overemphasized. The JT effect is indispensable for explaining the multiplet ground level; a vanishing JT effect yields a singlet ground state in contradiction with the experimental specific heat data. The JT effect results in inequivalent Cr centers. We note that for all the other DMS, the JT effect is less important, since it affects the ground term of the magnetic ion only very weakly.

The equilibrium model for a macroscopic crystal describes reasonably well the observed specific heat and the magnetization. For the magnetization, the magnetization anisotropy observed at low temperatures is described only qualitatively, which suggests a deviation from a true equilibrium distribution of different Cr centers. Due to the low Cr concentrations in the present samples, no effects of Cr-Cr coupling were observed.

ACKNOWLEDGMENTS

We acknowledge financial support from The State Committee of Scientific Research (Poland) Grant No. 2 P302 260 03, NSF (U.S.A.) Grant No. DMR-9221141, and the Royal Academy of Arts and Sciences (The Netherlands).

APPENDIX

We chose each wave function Ψ to be a products of an orbital function ϕ and a spin function χ: $\Psi = \phi\chi$. The five orbital functions we used, diagonalize $\mathcal{H}_{cf}$.[12] The functions are

$$\begin{aligned}
\phi_1 &= (|\,2,2\rangle + |\,2,-2\rangle)/\sqrt{2},\\
\phi_2 &= |\,2,0\rangle,\\
\phi_3 &= (|\,2,2\rangle - |\,2,-2\rangle)/\sqrt{2},\\
\phi_4 &= |\,2,1\rangle,\\
\phi_5 &= |\,2,-1\rangle,
\end{aligned} \tag{A1}$$

where $|\,a,b\rangle$ denotes $|\,L=a,L_z=b\rangle$. The spin functions were selected to have the simple form $\chi = |\,S=2,S_z\rangle$, with $S_z = 2,1,0,-1,-2$.

The functions ϕ_1 and ϕ_2 form the basis for the E representation of the T_d group, whereas ϕ_3, ϕ_4, and ϕ_5 form the basis for the T_2 representation. The energies corresponding to the eigenfunctions (A1) are: $E_{1,2} = 72B_4$ and $E_{3,4,5} = -48B_4$.[12] The crystal-field splitting, conventionally defined as $\Delta = 10Dq$, is, therefore, $120B_4$. In the case of Cr^{++}, the ground term is an orbital triplet $^5T_2$, contrary the situation for Fe ion , where the sequence $^5T_2$, ^5E was reversed.[13,14] This reversed sequence marks the difference between Fe and Cr ions. The E term is rather insensitive to the JT effect,[23] and, therefore, magnetic properties of Fe^{++} ions, which result from the spin-orbit split ^5E term, can be described using a simple crystal-field model which neglects the JT effect.[5,19]

The Hamiltonian $\mathcal{H}_d$ associated with the tetragonal distortion (representing the static Jahn-Teller effect) is also diagonalized by wave functions (A1). The energies are the following:[12]

$$\begin{aligned}
E_1^d(\phi_1) &= +6B_2^0 + 12B_4^0,\\
E_2^d(\phi_2) &= -6B_2^0 + 72B_4^0,\\
E_3^d(\phi_3) &= +6B_2^0 + 12B_4^0,\\
E_4^d(\phi_4) &= -3B_2^0 - 48B_4^0,\\
E_5^d(\phi_5) &= -3B_2^0 - 48B_4^0,
\end{aligned} \tag{A2}$$

where B_2^0 and B_4^0 are the parameters of $\mathcal{H}_d$. The total energy scheme is given in Fig. 7(a).

The basis Ψ_i, where $i = 1,\ldots,25$, was used to calculate the matrix elements of the spin-orbit interaction and the Zeeman term.

[1] *Diluted Magnetic Semiconductors*, edited by J. K. Furdyna and J. Kossut (Academic Press, New York, 1988), Vol. 25; *Diluted Magnetic Semiconductors*, edited by M. Balkanski and M. Averous (Plenum Press, New York, 1991); J. Kossut and W. Dobrowolski, in *Handbook of Magnetic Materials*, edited by K. H. J. Buschow (North Holland, Amsterdam, 1993), Vol. 7, p. 231.

[2] A. Twardowski, Phys. Scr. **T39**, 124 (1991).

[3] W. J. M de Jonge and H. J. M. Swagten, J. Magn. Magn. Mater. **100**, 322 (1991).

[4] A. Twardowski, H. J. M. Swagten, and W. J. M. de Jonge, in *II-VI Semiconducting Compounds*, edited by M. Jain (World Scientific, Singapore, 1993), p. 27.

[5] A. Twardowski, J. Appl. Phys. **67**, 5108 (1990); A. Twardowski, in *Diluted Magnetic Semiconductors* (Ref. 1).

[6] A. Twardowski, T. Fries, Y. Shapira, P. Eggenkamp, H. J. M. Swagten, and M. Demianiuk, J. Appl. Phys. **73**, 5745 (1993).

[7] W. Mac, Nguyen The Khoi, A. Twardowski, J. A. Gaj, and M. Demianiuk, Phys. Rev. Lett. **71**, 2327 (1993).

[8] J. T. Vallin, G. A. Slack, S. Roberts and A. E. Hughes, Phys. Rev. B **2**, 4313 (1970).

[9] J. T. Vallin and G. D. Watkins, Phys. Rev. B **9**, 2051 (1974).
[10] M. E. Lines and J. V. Waszczak, J. Appl. Phys. **48**, 1395 (1977); Y. Shapira (unpublished).
[11] A. Twardowski, H. J. M. Swagten, and W. J. M. de Jonge, Phys. Rev. B **42**, 2455 (1990).
[12] A. Abragam and B. Bleaney, *Electron Paramagnetic Resonance of Transition Ions* (Clarendon Press, Oxford, 1970), p. 372.
[13] G. A. Slack, S. Roberts, and J. T. Vallin, Phys. Rev. **187**, 511 (1969).
[14] W. Low and M. Weger, Phys. Rev. **118**, 1119 (1960).
[15] J. T. Vallin and G. D. Watkins, Solid State Commun. **9**, 953 (1971).
[16] B. Nygren, J. T. Vallin, and G. A. Slack, Solid State Commun. **11**, 35 (1972).
[17] A. E. Hughes and J. T. Vallin (unpublished) (see also Refs. 8 and 9).
[18] A. Twardowski, K. Pakula, I. Perez, P. Wise, and J. Crow, Phys. Rev. B **42**, 7567 (1990).
[19] H. J. M. Swagten, A. Twardowski, W. J. M. de Jonge, and M. Demianiuk, Phys. Rev. B **39**, 2568 (1989).
[20] A. Twardowski, H. J. M. Swagten, W. J. M. de Jonge, and M. Demianiuk, Phys. Rev. B **44**, 2220 (1991).
[21] R. Krevet, A. Twardowski, M. von Ortenberg, W. Mac, and M. Demianiuk, Solid State Commun. **87**, 709 (1993).
[22] W. Mac, R. Krevet, A. Twardowski, M. von Ortenberg, and M. Demianiuk, Physica B (to be published).
[23] J. T. Vallin, Phys. Rev. B **2**, 2390 (1970); E. E. Vogel and J. Rivera-Iratchet, *ibid.* **22**, 4511 (1980); K. Lebecki and A. Twardowski, Solid State Commun. **80**, 377 (1991).
[24] The anisotropy of energy levels depends not only on the angle α between **B** and the distortion axis, but also on the orientation of B in the plain perpendicular to the distortion axis. The latter dependence is, however, rather weak.